www.amlett.org, www.amlett.com, DOI: 10.5185/amlett.2012.7396 Published online by the VBRI press in 2013

Equivalent circuit models and analysis of impedance spectra of solid electrolyte $Na_{0.25}Li_{0.75}Zr_2(PO_4)_3$

U. Ahmadu[1*], Ŝ.Tomas[2], S. A. Jonah[3], A. O. Musa[4], N. Rabiu[5]

[1]*Department of Physics, Federal University of Technology, Minna, Nigeria*
[2]*Faculty of Physics, Vilnius University, Lithuania*
[3]*Centre for Energy Research and Training, Ahmadu Bello University, Zaria, Nigeria*
[4]*Department of Physics, Bayero University, Kano, Nigeria*
[5]*Department of Physics, Ahmadu Bello University, Zaria, Nigeria*

[*]Corresponding author. E-mail: u.ahmadu@yahoo.com

Received: 25 July 2012, Revised: 15 August 2012 and Accepted: 15 August 2012

ABSTRACT

Two RC model circuits are connected in series in order to analyze the electrical and dielectric behaviour of mixed alkali $Na_{0.25}Li_{0.75}Zr_2(PO_4)_3$ NASICON compound. However, the data obtained could best be described by one RC circuit representing the grain boundary resistance (R_{gb}) and capacitance (C_{gb}) in the temperature and frequency range 300-600 K and 300 kHz to 1GHz, respectively. The values of the grain boundary activation energy E_{gb} obtained by fitting to the Arrhenius equation in a z'', z' plot is ~ 0.40 eV, which is close to the bulk activation energy $E_b \sim 0.36\ eV$ for electrical conduction. The maximum conductivity obtained is 0.3 S/m at 590 K. A non Debye character was observed in the dielectric permitivity ε' in its frequency dependence. However, the temperature dependence of ε' followed a linear behaviour at low temperatures and frequencies but decreased at higher temperatures. Complex non linear least squares fitting of impedance data using a composite circuit shows good fitting results with relative standard deviation less than 0.2 for all the free parameters which is indicative of the accuracy of data obtained. Similar good fitting results, using a generic battery model, suggest the applicability of the material in rechargeable lithium ion batteries. Copyright © 2013 VBRI press.

Keywords: NZP; impedance spectroscopy; electrical conductivity; dielectric relaxation; equivalent circuit.

S. A. Jonah graduated from the University of Ilorin in 1983. Professor Jonah joined the services of Ahmadu Bello University in 1985 and rose to the rank of Professor of Nuclear Physics in 2004. Professor Jonah has participated in several Conferences, Workshops, Technical Meetings and Research Coordination Meetings in Austria, Australia, Cameroon, China, Czech Republic, Ghana, Egypt, Jamaica, Morocco, South Africa, and USA. He won the International Atomic Energy Agency's (IAEA) Research Grants in 1996, 2005, 2006 and 2008, as well as the University of Chicago, USA research grant 2010. Professor Jonah has also served as an expert of the IAEA to China Institute of Atomic Energy in 2007 and Ghana Atomic Energy Commission in 2008. He was at the Abdus Salam International Centre for Theoretical Physics, Trieste (ICTP), Italy in 2001, 2002 and 2003 and Visiting Scholar to the Nuclear Engineering Division, Argonne National Laboratory, USA in 2006 and 2010. Professor Jonah was invited to participate in the Fissile Material Working Group Meeting as an international expert at the World Nuclear Security Summit in Washington in April 2010. He has supervised several Ph. D. and M. Sc students and served as external examiner in Nigeria and Ghana. Professor Jonah has published his research findings in over 50 journal articles, mainly in high impact factor international journals and has served as peer reviewer for Applied Radiation and Isotopes and Annals of Nuclear Energy, published by Elsevier. He was the Reactor Manager and Head of Reactor Engineering Section.

Ŝ. Tomas received his Ph.D. in 2009 from Vilnius University (Lithuania) under the supervision of Professor Antanas Feliksas Orliukas for work on the analysis of lithium and oxygen vacancy conducting superionic materials with impedance spectroscopy. He was a postdoctoral fellow in Universite du Maine (France) in 2010. Since 2011 T. Salkus is working at Vilnius University and in 2012 he received postdoctoral followship from Research Council of Lithuania ("Postdoctoral Fellowship Implementation in Lithuania" project).

N. Rabiu born in Charanchi, Charanchi local Government, Katsina State Nigeria. He joined the services of Ahmadu Bello University, Zaria, Nigeria as Graduate Assistant in September, 1989. He had his master's and doctorate degrees in physics in 1994 and 2005 respectively from the same University. He has held many positions in the University which include Head of Department of Physics, Assistant Dean of the faculty of Science, Faculty Examination Officer, Chairman of Academic Staff Union of Universities, Ahmadu Bello University Branch among others. Due to share hard work and commitment, he rose from the rank of Graduate Assistant to an associate Professor in 2009. He has supervised many PhD and M.Sc degrees and

currently has over twenty five publications in local and international journals and is an external examiner to undergraduate and postgraduate students in many universities in Nigeria.

Introduction

In recent times, based on scientific relevance and technological applications, various classes or families of materials have been investigated and characterized by different techniques for different applications, depending on the nature of the study and purpose inview. The Perovskite family, for example, has been widely studied for their high dielectric and ferroelectric properties in different temperature and frequency ranges, upto about 10 MHz and ~700 K [**1**] $Ba(Fe_{0.5}Nb_{0.5})O_3$-$BaTiO_3$; [**2**] $(Bi_{0.5}Na_{0.5}Na_{0.5})_{1-x}Ba_xTiO_3$. Similar studies have been carried out on other compositions in this family by some workers [**3**] (1-x) $BaTiO_3$-xPZT(65/35)]; [**4**] (1-x)$Ba(Fe_{0.5}Nb_{0.5})O_3$-x$BaTiO_3$; [**5**] $Bi(Mg_{0.5}Ti_{0.5})O_3$-$PbTiO_3$ and [**6**] $(K_{0.5}Bi_{0.5})(Fe_{0.5}Nb_{0.5})O_3$. In each of these studies, dielectric behaviour, electrical conductivity and their mechanisms have been analysed, using equivalent circuits in some cases.

The Pyrochlore family of compounds have also been investigated and reported for their luminiscence behaviour [**7**] using Eu, Dy co-doped $Y_2Zr_2O_7$. In a similar manner [**8**] have studied the dielectric and electrical conductivity properties of $Dy_2(Bo_{0.5}R_{0.5})_2O_7$, where R=W, Mo). The study of wear behaviour of the alloy Al-12Si and Al-12Si-Sn/$ZrSiO_4$ at different loads and temperatures have been investigated and reported by [**9**]. The compound $Ba_3Sr_2GdTi_3V_7O_{30}$ belonging to the Tungsten Bronze family has been shown to have a dielectric anomally related to a ferroelectric phase transition [**10**].

As a result of the enormous advantages of increased efficiency of performance and miniaturization based on size–scaling, most materials are now prepared at the nanoscale level for a wide range of applications and across interdisciplinary borders. A foremost objective of such research is that of development of intelleignt nanomaterials which envision additional functionalities built into the molecular structure of the materials such that a desirable response occurs under specified conditions [**11**].

An outstanding example of another versatile material in terms of its diverse applications is NZP (sodium zironium phosphate) family of compounds with formula $NaZr_2(PO_4)_3$. Series of isostructural compounds have been synthesised from NZP leading to the compositions generally referred to as NASICON, sodium superionic conductor ($Na_{1+x}Zr_{2-x}Si_xP_{3-x}O_{12}$, where x = 0-3). NZP has diverse potential applications based on its unique structure, in environmental gas sensors, thermal expansion [**12**], nuclear waste immobilization [**13,14**] and rechargeable lithium ion batteries, to name but a few. These applications are dependent upon special structural features of NASICON. All the elements in NZP can be substitutted (except Oxygen) by atoms of different sizes and oxidation states, thereby confering on the compositions varying physical and chemical properties but with the same crystal system. NZP and NASICON have been synthesized principally using the solid state reaction method with the concomitant precipitation of ZrO_2 [**15**] produced as a result of the high temperature reguired in its synthesis. There have been reports of impurity phases detected in their synthesis by some workers [**16-18**]. $Na_{1-x}Li_xZr_2(PO_4)_3$ (where x = 0.0, 0.3, 0.5, 0.7 and 1.0) have been studied by solid state reaction and characterized by X-ray diffraction and differential thermal analyses (DTA) [**19**]. However, the conductivity of the base compound $NaZr_2(PO_4)_3$ has been reported to be very low, below the applicable range and has poor sinterability [**20**]. Thus most studies have been carried out on partial as well as full substitutions of Na, Zr and P by higher valent elements of different radii [**21-23**] in order to improve the conductivities of the compositions. Such substitutions have lead to an enhancement of electrical conductivity [**24, 25**].

We have investigated the synthesis [**26**] and the electrical and dielectric permitivity ε' of $Na_{0.25}Li_{0.75}Zr_2(PO_4)_3$ mixed ionic conductor . Our earlier investigations based on impedance spectra, dielectric and conductivity analysis revealed a Debye-like character, and a relaxation in the temperature dependence of the permitivity ε' at low frequencies with peaks at ~ 469 K [**27**]. In the current work we analyze the electrical and dielectric properties of the compound based on equivalent circuit analyses theoretically, using composite electric circuit in complex non linear least squares and generic battery model fitting procedures and determine the mechanisms involved in order to evaluate its suitability for application as solid electrolyte. The structure, electrical and dielectric behaviour of the compound has not been reported from our investigations. Moreover, analyses based on complex non linear least squares fitting and generic battery models have also not been reported for this compound. Hence analysis and deductions will be based on compounds of the same family generally. Further, the characterization of this family of compounds using the Gigahertz technique is novel as very few works have been reported in this respect [**28**]. Because of the scientific challenges in the understanding of the electrical and dielectric behaviour and its technological importance for numerous applications, the results of this investigation are presented.

Experimental

Synthesis and characterization

Starting materials of analytical grade of purity $> 99\%$ were used, $Na_2CO_3.H_2O$, ZrO_2, Li_2CO_3 and $NH_4H_2PO_4$ (all from BDH, British Drug House, U.K.). Stoichiometric amounts of these materials were mixed and thoroughly ground in an agate mortar for about five hours. The sample was heated at temperatures from 573 to 1523 K successively, using standard solid state reaction method. Full details of experimental procedure have been described in our earlier works [**26, 27**]. Briefly however, X-ray diffraction (XRD) measurements were carried out using a precision mini XRD diffractometer MD-10, Version 2.0.4 by Radicon Ltd in the 2θ range 16-70^o at a working power of 25 kV, using 20 minutes acquisition time and CuKα radiation λ =1.5406 Å at a scan rate of 0.05^o in other to ensure that the compound is single phase. However, minor phase of $Na_5Zr_2(PO_4)_3$ and ZrO_2 were detected. ZrO_2 is characteristically observed in solid state reactions due to the high temperature used in its synthesis. The SEM

micrograph of fractured surfaces of sintered specimen was obtained using a TMEC Scanning Electron Microscope (SEM) working at 5 kV. **Fig. 1** depicts the micrograph of the fractured surfaces of well-structured grains of $Na_{0.25}Li_{075}Zr_2(PO_4)_3$ with an average grain size of ~2-5 µm with small porosity. The theoretical density obtained by measurement of the pellet's dimensions was ~ 88%. The small whitish grains are the $Na_5Zr(PO_4)_3$ detected in the XRD. Pellets with dimensions (electrode surface area) 9.08 mm^2 and length 1.5 mm and sintered at the maximum temperature of 1523 K using a die of 8 mm at 300 MPa pressure were used for the electrical measurements. The control and acquisition of data were carried out automatically using MathLab software on an Agilent Network Analyser E5062A, in the frequency and temperature range 300 kHz to 1 GHz and 310-600 K, respectively. Measurements were performed every 10 K, on heating the sample at 1 K per min using a voltage of 200 mV.

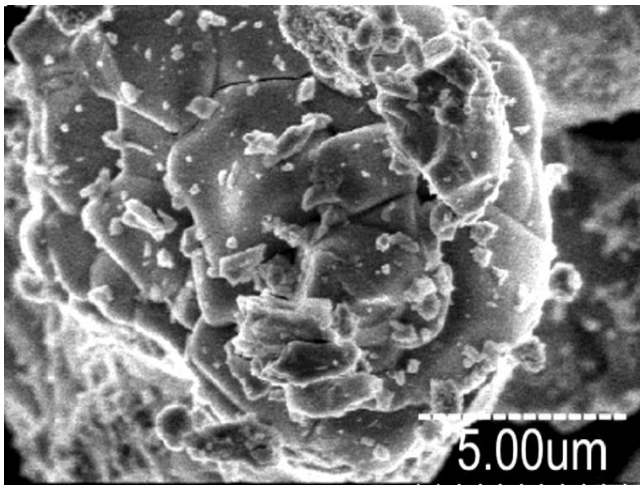

Fig. 1. Micrograph of the fractured surfaces of well-structured grains of $Na_{0.25}Li_{075}Zr_2(PO_4)_3$ with average grain size of ~2-5 µm.

Results and discussion

Impedance analysis

The compelx impledance of materials can be obtained from $\frac{V^*}{I^*}$, where V^* and I^* are the applied voltage and current, respectively. The complex electric modulus M^* and the complex permitivity ε^* can be calculated as follows:

$$M^* = M' + iM'' = i\omega C_o Z^* \quad (1)$$

$$\varepsilon^* = \varepsilon' - i\varepsilon'' = \frac{1}{i\omega C_o Z^*} \quad (2)$$

where $\omega = 2\pi f$ is the angular frequency, $i = \sqrt{(-1)}$, $C_o = \varepsilon_o \frac{S}{d}$ is the empty cell capacitance, S is the sample area and the d is the thickness of the sample.

The complex plane plots (Z'' vs Z') at different temperatures have been presented in fig. 2. The angular frequency ω increases in an anticlockwise manner on the Z' axis. Two semicircular arcs are observed in the temperature range 450-600 K with the arcs becoming smaller with increase in temperature and shrinking from right to left of the Z' axis. This implies a reduction in the diameters of the arcs which results in an increase in electrical conduction due to reduction in resistance of the sample. It is observed that the peak intensity (Z'') of one of the arcs is dominant, while the other with a smaller diameter has smaller peak intensities which lie outside the frequency range of investigation as the temperature increases. The ratio of the diameter of the small arc to the big one is very small, of the order of 0.33 at 310 K and 0.51 at 500 K. This indicates that the resistance of the big arc is much greater than the small arc as both shift from right to left on the axis as the temperature increases due to the decrease of impedance. At lower temperatures (310-400 K) however, we find that the arc formation is poor due to their overlap, as shown in the inset of **Fig. 2**.

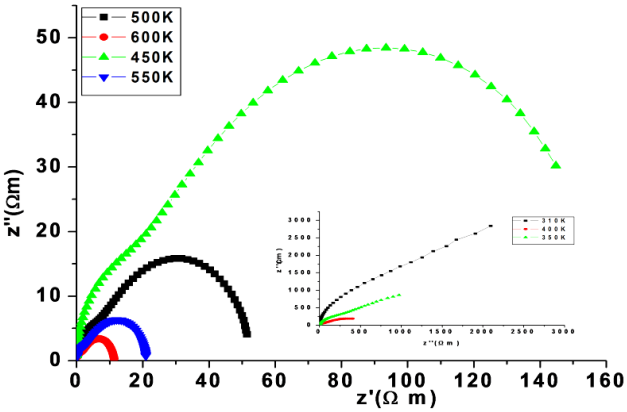

Fig. 2. Complex plane plots (Z'' vs Z') at different temperatures .

In **Fig. 3a** we show the frequency dependence of the imaginary part of impedance (Z'') at different temperatures. Only one prominent peak is observable at each temperature and it systematically shifts towards higher frequencies with increase in temperature after an initial decrease. This implies a thermal activation of the conductivity relaxations which are within a decade of frequency ($1.55 \cdot 10^7 - 2.32 \cdot 10^6$ Hz) in the temperature range 470-490 K. In the case of the linear plot of Z'' vs Z', the conduction process results in a semicircular arc. However, a log-log plot, like that shown in **Fig. 3b**, enables one to compare the two responses (grain and grain boundary, depicted by the small vs big arcs, respectively) that have vastly different impedances in one plot. Although the semicircular arcs become distorted, logarithmic plots offer significant advantages in many ways. In fig. 3a which is plotted in the temperature range 310-600 K, prominent peaks can be seen (indicated by arrows) in the lower frequency range which succesively shift toward higher frequencies as the temperature increases (400-600 K).The small arcs, especially at 400-500 K, can be attributted to grain boundary and grains (bulk) respectively, due to the frequencies and capacitances of these peaks as explained

below. The fact that the resistance associated with the big arc is much bigger than the small arc is further reason to make this association.

Analysis of impedance spectra can be modelled based on an equivalent electric circuit consisting of a resistor (R) and capacitance (C) elements. Polycrystalline materials are known to exhibit intergrain and grain boundary impedances and thus they can be represented by the equivalent circuit shown in **Fig. 3c**. We have used this model to theoretically analyze our sample's electrical behaviour. The circuit has two RC elements joined together in series representing the grain ($R_g C_g$) and grain boundary ($R_{gb} C_{gb}$). Each of the subcircuits consists of a resistor and capacitor joined together in parallel and the impedance of the circuit shown in fig. 3c can be represented by,

$$Z^* = \frac{1}{\frac{1}{R_g} + i\omega C_g} + \frac{1}{\frac{1}{R_{gb}} + i\omega C_{gb}} = Z' - iZ'' \quad (3)$$

where

$$Z' = \frac{R_g}{1+(\omega R_g C_g)^2} + \frac{R_{gb}}{1+(\omega R_{gb} C_{gb})^2} \quad (4)$$

and

$$Z'' = R_g \left[\frac{\omega R_g C_g}{1+(\omega R_g C_g)^2}\right] + R_{gb} \left[\frac{\omega R_{gb} C_{gb}}{1+(R_{gb} C_{gb})^2}\right] \quad (5)$$

Eq. (5) can be applied to the response peaks of the grain and grain boundaries located at $\frac{1}{2\pi R_g C_g}$ and $\frac{1}{2\pi R_{gb} C_{gb}}$, respectively. The frequency of the peaks in the Z'' vs Z' plots were deduced based on the conditions $\omega\tau = 1$, $RC = \tau$ and $\omega = 2\pi f$, which give $f = \frac{1}{2\pi RC}$, where ω is the angular frequency and τ is the relaxation time. The peak values are found to be proportional to the associated resistances but in general the peak frequencies of the grain boundaries are lower than those of grains due to their large resistances and capacitances. This is why we attribute in the impedance spectra, the higher frequency response corresponding to the small arc in **Fig. 3a** to the grains and the lower ones to the grain boundaries. A comparison of the peak values of the responses show that the resistances of the grain boundaries below 400 K is at least five times bigger than that of the grains (i.e., $R_{gb} \gg R_g$), where R_g, R_{gb} were obtained by extrapolating the curvy portion of the arcs to the Z' axis.

In **Fig. 3a** and **3b**, the response peaks from the grains are too weak to be analyzed by **Eq. (5)** and some of them lie beyond the frequency range of investigation. At lower temperatures the grain boundary peaks are inaccessible but move into the frequency range of investigation when the temperature increases, while at the same time the grain peaks move out. We can approximately fit the Z'' to a single $R_{gb} C_{gb}$ parallel circuit instead. Thus for an ideal $R_{gb} C_{gb}$ parallel circuit the electrical response of the system is of the Debye-type given by,

$$Z'' = \frac{R_{gb}}{1+i\omega R_{gb} C_{gb}} \quad (6)$$

Moreover, it has been observed that for real materials Z'' is better described using the Cole–Cole equation for polycrystalline materials,

$$Z'' = \frac{R_{gb}}{1+(i\omega\tau_{gb})^{\alpha}} \quad (7)$$

where $\tau_{gb} = R_{gb} C_{gb}$ and the parameter $\alpha, 0 < \alpha \leq 1$ is used to measure the departure from the ideal Debye response. In essence this implies that the grain boundary response is not of the ideal RC elements. It is found that τ_{gb} corresponds to relaxation times which reduce from $3.39 \cdot 10^{-7}$ s at 400 K to $7.65 \cdot 10^{-9}$ s at 600 K, corresponding to capacitances of $1.17 \cdot 10^{-9}$ F and $1.1 \cdot 10^{-8}$ F, respectively.

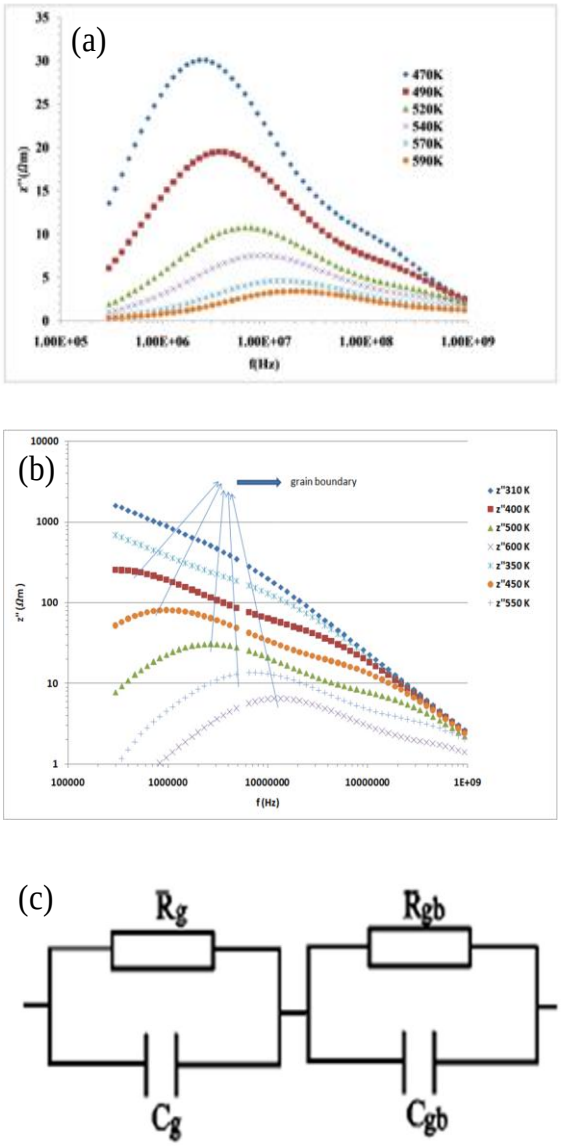

Fig. 3. (a) Frequency dependence of imaginary part of impedance (Z'') at different temperatures, (b) Log-log plot of Z'' vs f showing the grain boundary responses indicated by an arrow and (c) Equivalent circuit representation of polycrystalline materials with grain and grain boundary impedances.

In **Fig. 4** the natural logarithm of the relaxation frequencies ($ln\ f_{gb}$) at different temperatures have been plotted against reciprocal temperature for the grain boundary. It is found that it can be fitted to the Arrhenius equation of the form $f_{gb} = f_o \exp\left(-\frac{E_{gb}}{kT}\right)$, where f_o is the preexponential factor, E_{gb} is the activation energy for relaxation of grain boundary, k the Boltzman constant and T the absolute temeperature. The solid line in **Fig. 4** represents the fit to the equation (the goodness of fit is ~ 0.999) while the dots are the actual data points. From the slope of the graph the value of $E_{gb} \sim 0.40\ eV$. **Fig. 5** shows the plot of the bulk and total dc conductivities (σ_b ,σ_t), respectively, plotted against reciprocal temperature. These values were obtained by extrapolation of the curvy part of the arcs to the z' axis in order to obtain the resistances calculated based on the geometrical dimensions of the samples. The plots also show a good fit to the Arrhenius equation which can be written in the form (for both) $\sigma_{b,t} = \sigma_{ob,\ ot} \exp\left(-\frac{E_{b,t}}{kT}\right)$, where $\sigma_{b,t}$ are the bulk and total conductivities (bulk and grain). $\sigma_{ob,ot}$ represents the preexponential factors for each case and $E_{b,t}$ are the activation energies for the grain and total conductivities. The plots in **Fig. 5** are represented by ln σ_b(lnsigb), ln σ_t (lnsigt) vs 1/T as indicated by the legends on the plots. The solid lines represent the fit to the Arrhenius equation. The computed values of $E_{b,t}$ from the slopes of the solid lines are ~ 0.36 eV and 0.41 eV, respectively. This implies that E_{gb} is ~ 0.40 eV and that bulk conductivities are similar and indicate a similar conduction mechanism for both dc and relaxation, pointing to a weak temperature dependence of capacitance. It has been reported [29] that a maximum dc conductivity value of ~ 0.27 S/m at 623 K was obtained in the series $AgTaYP_3O_{12}$, with the lowest reported activation energy of ~ 0.43 eV for the series $AgTaCrP_3O_{12}$. These values are in close agreement with our results and are typical for this family of compounds.

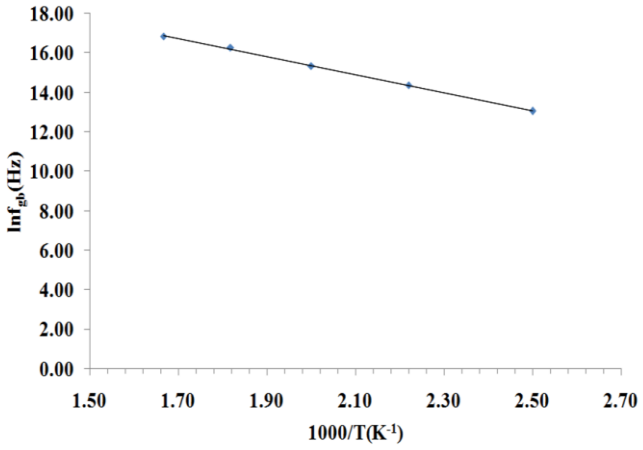

Fig. 4. Plot of relaxation frequencies ($ln\ f_{gb}$) at different temperatures against reciprocal temperature for the grain boundary.

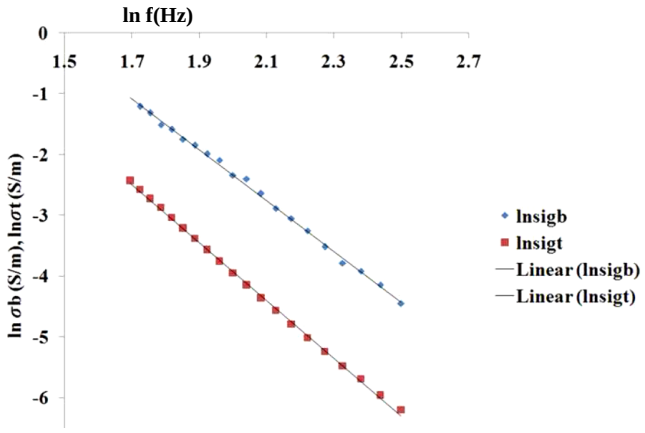

Fig. 5. Plot of bulk and total dc conductivities (σ_b ,σ_t) plotted against reciprocal temperature.

AC conductivity analysis

Fig. 6a is a log-log plot of the ac conductivity versus frequency in the temperature range 310-600 K. The ac conductivity of ionic materials at a given temperature is usually described by the power law equation:

$$\sigma_{ac} = \sigma_{dc} + A\omega^n, \quad (8)$$

where σ_{dc}, is the extrapolated conductivity value of the frequency (at $\omega = 0$) independent region, A is the ac coefficient, n the correlation exponent of the ions and $\omega = 2\pi f$, where f is the frequency. The crossover point of the frequency independent plateau and the high frequency ac dispersive region are shifted toward the high frequency values with increasing temperature. This can be explained by the fact that with increase in T, the kinetic energy of the ions also increases and hence their vibrational frequency. The onset part of the conductivity dispersion at different temperatures are found to lie on a straight line, implying that σ_{dc}(T) and the onset frequency $f(T)$ are proportional to eachother and both are thermally activated with almost the same energy of activation, indicative of a general feature of the power law proposed by Jonscher **[18]**.

From the slope of ln σ_{ac} vs ln f we determine the value of the correlation exponent n which increases with increase in temperature in a narrow range (0.148-0.254) and shows that n is a temperature and frequency dependent relaxation process. The plot of n versus T at different temperatures is shown in **fig. 6b** with the linear fit in solid line. Some workers **[16, 30]** have reported values of n in the range 0.6-0.9 for different compositions in their study of $Na_{1+x}Ti_{2-x}Al_x(PO_4)_3$ (x= 0.6-0.9) and $Li_{1+x}[(Ta_{1-2x}Ge_x)](PO_4)_3$ respectively. However, the workers **[30]** could not explain the high value of 0.9 obtained for low compositions x = 0.0 and 0.3. Our current values are very low and thus deserve further investigations. The values of σ_{dc} increase with rises in temperature from ~ $2 \cdot 10^{-3}$ to $4.98 \cdot 10^{-2}$ S/m between 400-550 K and reached ~ 0.1 S/m at 600 K and is comparable to the value of 0.3 obtained for the dc values from impedance measurements.

Also some workers have reported **[29]** a value of $\sigma_{dc} \sim 6.88 \cdot 10^{-5}$ S/m at 373 K with corresponding activation energy of 0.49 eV for $AgTaYP_3O_{12}$. Our results therefore show a significant enhancement. In 'order to ascertain the electrical conduction mechanism of materials, different theoretical models **[31]** have been proposed such as the classsical hopping mechanism which seems suitable to explain the observed conduction mechanism. On the otherhand, Quantum Mechanical Tunnelling (QMT) model, where the exponent n is slightly less than 0.8 and increases slightly with temperature **[32]** does not perfectly fit our data due to the low value of n obtained.

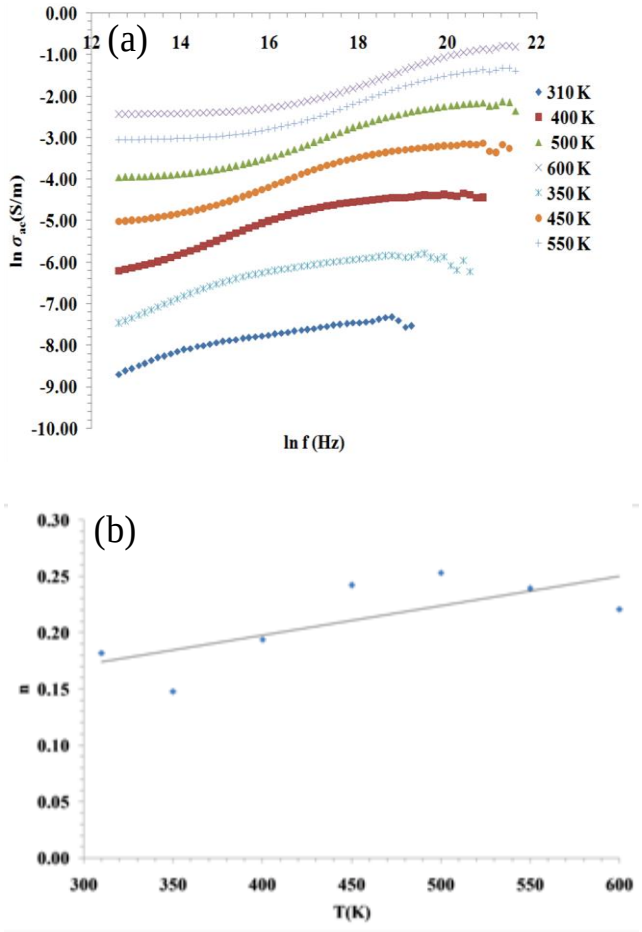

Fig. 6. Log-log plot of (a) ac conductivity versus frequency in the temperature range 310-600 K and (b) correlation exponent n versus T at different temperatures with linear fit in solid line.

Modulus formalism

We have explained earlier in the analyses that the peak intensities arising from grains (z'') are very weak due to the small resistances of the grains in comparison to the grain boundaries. We can however enhance this effect for better analyses when viewed from the electric modulus formalism ($M^* = M' + iM''$). The complex modulus M^* is now generally used in conjunction with the impedance and permitivity formalisms to distinguish between grain and grain boundary effects and also to understand the miscroscopic phenomena responsible for local dielectric relaxations and electrical conductivity.

Starting from Eq. (1) and (3), the electric modulus represented by the circuit in **Fig. 3c** is,

$$M' = \frac{C_o}{C_g}\left[\frac{(\omega R_g C_g)^2}{1+(\omega R_g C_g)^2}\right] + \frac{C_o}{C_{gb}}\left[\frac{(\omega R_{gb} C_{gb})^2}{1+(\omega R_{gb} C_{gb})^2}\right] \quad (9)$$

and

$$M'' = \frac{C_o}{C_g}\left[\frac{\omega R_g C_g}{1+(\omega R_g C_g)^2}\right] + \frac{C_o}{C_{gb}}\left[\frac{\omega R_{gb} C_{gb}}{(\omega R_{gb} C_{gb})^2}\right] \quad (10)$$

Eq. (10) shows that there is relaxation in the M'' representation. Similar to the z'' representation, the response peaks for the grains and grain boundaries also occur at frequencies $\frac{1}{2\pi R_g C_g}$ and $\frac{1}{2\pi R_{gb} C_{gb}}$, respectively. Since the peak intensities are proportional to the reciprocals of the associated capacitances, the smaller capacitances therefore dominate in the modulus plots. It has been reported that the grains usually have smaller capacitances than the grain boundaries **[33]** which make their response peaks stronger in the spectra.

In **Fig. 7a** the frequency dependence of M'' at different temperatures has been plotted. The relaxation frequencies shift to higher frequencies with increase in temperature while the peaks of M'' slightly increase with increase in temperature showing that the capacitances of the grain and grain boundaries are only slightly dependent on temperature. Further, there are no other peaks visible in the frequency range investigated and those outside the frequency range would be substantially smaller, implying that these frequencies are representative of the grains based on their higher relaxation frequencies which are in the range $1.12 \cdot 10^6$ to $6.95 \cdot 10^8$ Hz between 310-600 K. The peaks also seem to be broader than predicted by the ideal Debye behaviour (this should be expected since the RC elements are not ideal). The broadenings have been attributed to non exponential processes such as correlation between diffusive motions of ions and non uniformities in material microstructure which can further lead to spatial distributions of local conductivities and electrical response times **[34].**

Typical complex plane plots of M'' vs M' are shown in **Fig. 7b** and **7c** at 310 K and 600 K, respectively. A prominent arc at 310 K is shown in **Fig. 7b** which is gradually enhanced into a semicircular arc at 450 K. The arcs shift to the left with increase in temperature and the prominent peak is attributed to the small capacitance of the bulk compared to the grain boundary. It is observed that the grain boundary arc begins to appear at higher temperatures and their peaks are very much smaller than that of the bulk.

The arc shown in **Fig. 7b** at 310 K does not show any other peak that can be associated with the grain boundary at this temperature, though it began to appear at 350 K and is in fully formed at 600 K (**Fig. 7c**). Segments of the grain arc begin to disappear from the intersection on the M' axis with increase in temperature. The different capacitances of the grains and grain boundaries give rise to arcs of different diameters in the plots. The peak frequencies at which the maxima of M'' (f_{max}) occur correspond to those obtained

from the M'' vs f plot of **Fig. 7a**. The maxima of these peaks also conform to the condition $2\pi f_{max}\tau = 1$.

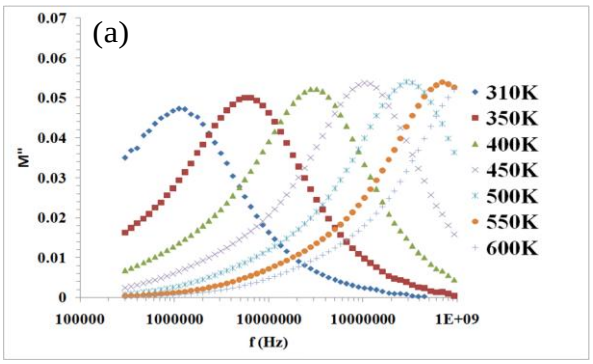

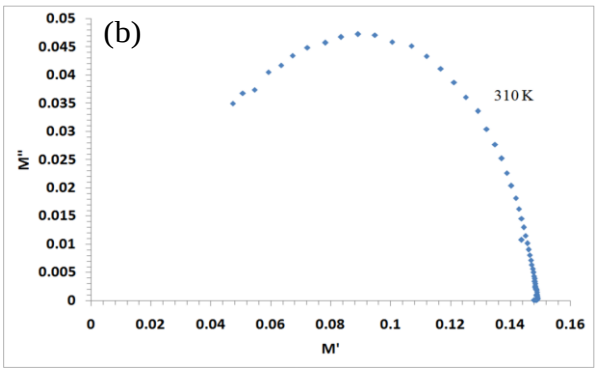

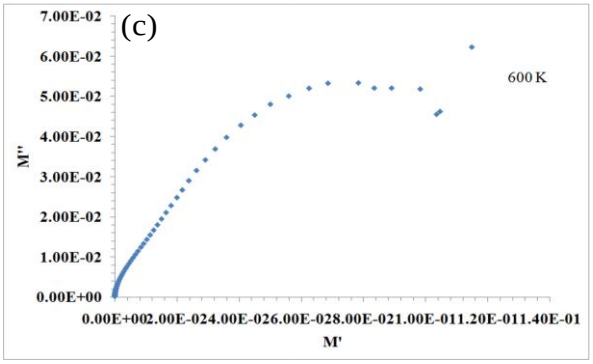

Fig. 7. (a) Plot of frequency dependence of M'' at different temperatures, (b) Complex plane plot of M'' vs M' at 310 K and (c) complex plane plot of M'' vs M' at 600 K.

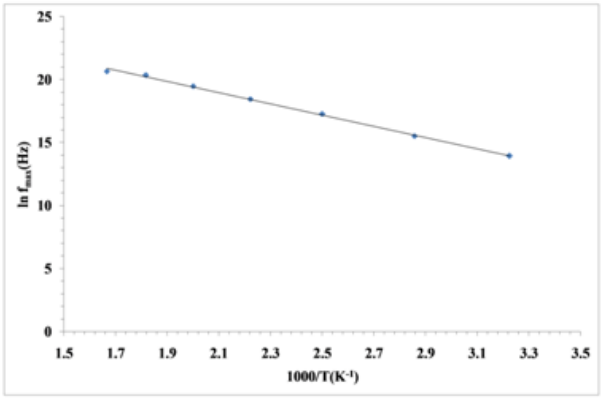

Fig. 8. Plot of ln f_{max} vs reciprocal temperature. The straight line is the linear fit to the Arrhenius equation.

A plot of ln f_{max} vs reciprocal temperature shown in **Fig. 8** shows that it also obeys the Arrhenius law. The solid line represents the fitting to the Arrhenius equation and its goodness of fit is ~ 0.999. The activation energy obtained from the slope is E_{fmax} ~ 0.39 eV, which is similar to E_{gb} ~ 0.40 eV earlier obtained for the grain boundary. E_{max} can be attributted to the activation energy for relaxation in the bulk **[16]** and the conduction mechanisms in both bulk and grain boundary may be the same.

Fig. 9 shows the plot of Z'' vs log f at 450 K with inset showing M'' vs log f at the same temperature. A close examination of the Z'', M'' vs log f plots obtained at 450 K indicate departures from the ideal Debye behaviour. Similarly, the width of the Z' versus log f plot at half height is greater than 1.14 decades of frequency and the peaks of Z'' and M'' are not coincident and suggest a departure from the ideal Debye behaviour (ideal Debye behaviour is 1.14 decades difference). Further, it is observed that the Z'' and M'' plots are symmetric and the shifts in f_{max} and changes in the values of f_{max} suggest a variation in capacitance.

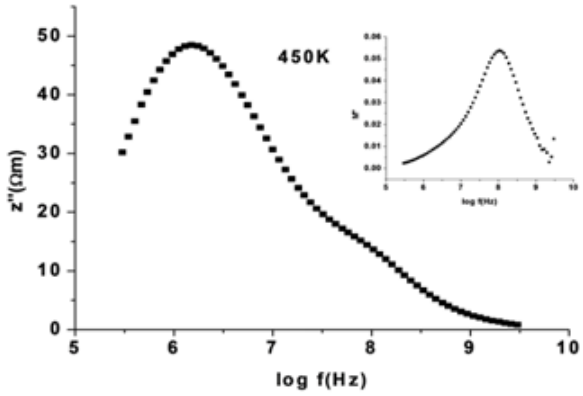

Fig. 9. Plot of Z'' vs log f at 450 K (inset is M'' vs log f plot at the same temperature).

Permitivity analysis

Fig. 10a shows the variation of real part of dielectric permitivity ε' against frequency in the temperature range 310-600 K. The dielectric constant response of a system is due to electronic, ionic, dipole and space charge polarizations. The space charge effects are negligible at very low temperatures and noticeable only in the low frequency region. For dielectric relaxation, the Cole–Cole equation $\varepsilon^* = \varepsilon'(\omega) - i\varepsilon''(\omega) = \varepsilon_\infty + \frac{\varepsilon_s - \varepsilon_\infty}{1+(i\omega\tau)^\gamma}$, where ε_s, ε_∞ are the static and high frequency limits of the dielectric constant, respectively, τ is the most probable relaxation time and γ is a constant with values between 0 and 1. In both ε' and ε'' no dielectric relaxations are observed in the frequency and temperature range investigated. At all the temperatures under investigation, ε' decreases with increase in frequency. The decrease is

significant especially at low frequencies which is asociated with the presence of mobile Li^+ and Na^+ ion polarization and dipole polarization, wheareas the increasing value of ε' at low frequencies is due to charge accumulation at the interface. It is observed that the low frequency dispersion of ε' gradually increases with increase in temperature due to an increase in the interfacial polarization as well as thermal activation associated with the mobile ions. The interfacial polarization is insignificant at high frequencies and hence ε' remains relatively constant **[35]**. At high frequencies ε' also decreases due to the high frequency of the field which reduces the contribution of the charge carriers toward the dielectric permitivity ε' and tends to a static value at all temperatures.

Fig. 10b shows the variation of imaginary part of dielectric permitivity (ε'') as a function of frequency in the temperature range 310-600 K. It is observed that ε'' decreases with increase in frequency at all the temperatures investigated. It has been generally postulated that the contribution to the dielectric loss consists of both the conduction and relaxation components. Thus the imaginary parts of dielectric loss have been explained based on the $\varepsilon'' = \frac{\sigma_{dc}}{\omega \varepsilon_o}$, where ε_o is vaccum dielectric constant, $\omega = 2\pi f$ is the frequency and σ_{dc} is the dc conductivity. The dc conduction leads to further dielectric loss in addition to that due to relaxation process. The higher value of ε'' at relatively low frequency may be attributted to the contribution arising from both the dc conduction and relaxation losses. At higher frequencies however, relaxation losses are the only sources of dielectric loss. We also notice that ε'' increases with increase in temperature because as the relaxation loss component reduces the conduction loss component increases more rapidly **[36]**. At all temperatures ε'' values approach a static value close to zero at higher frequencies.

The temperature dependence of ε' was also investigated in the temperature range 310-600 K and frequency range 0.3 MHz to 1 GHz as shown in **fig. 10c**. It is observed that at high frequency (1G Hz) the material shows an almost temperature-independent behaviour. Thus the capacitance of the bulk is almost independent of temperature and the slight increment observed is due to ion migration. There are no peaks observable either, resulting in non Debye behaviour which is in contrast to our earlier results **[27]**. It is possible that the ratios of the ions in this composition may be responsible for the absence of relaxation behaviour. Additionally, the peaks may not have been observed as a result of the frequency window which may be outside the frequency range in which the coupling of the ions is supposed to lead to relaxation **[36]**. At lower temperatures all the plots show a slow rise in ε' with increase in temperature, particularly at 0.3 and 0.54 MHz, and at higher frequencies, attaining a maximum value of ε' ~ 136 at 600 K . Some workers **[37]** have reported a value of $\varepsilon' \sim$ 17. 5 at 340 K for $Li_{1.3}Al_{0.15}Y_{0.5}Ti_{1.7}(PO_4)_3$ showing that the dielectric response is high compared to what has been reported for NASICON.

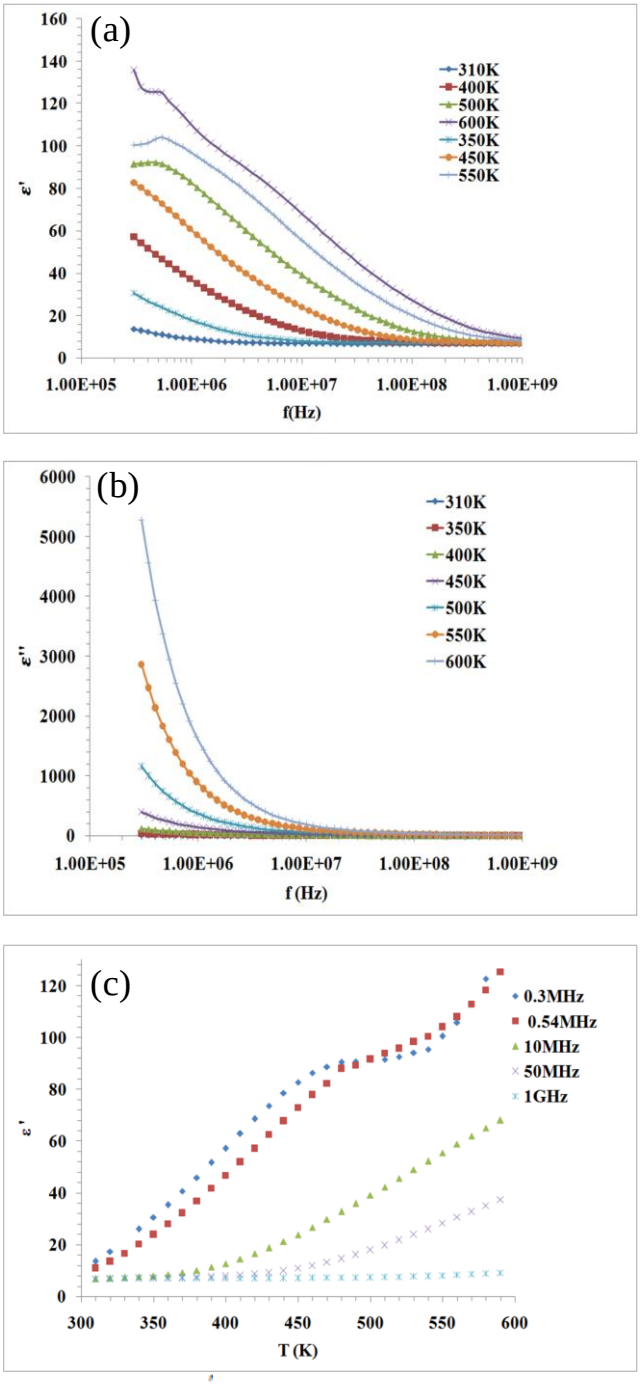

Fig. 10. (a) Plot of ε' against frequency in the temperature range 310-600 K, (b) Plot of ε'' vs frequency in the temperature range 310-600 K, and (c) Temperature dependence of ε' in the temperature range 310-600 K and frequency range 0.3 MHz to 1 GHz.

Complex non linear least squares fitting

The above theoretical analysis, which was based on approximation of the equivalent circuit was compared with the results from fitting the data using two Complex Non linear Least Squares fitting (CNLS) programs LEVM/LEVMW **[38]** and Multiple Electrochemical Impedance Spectroscopy Parameterization (MEISP) **[39]**. The impedance spectra at 600 K successfully fitted the 'O' equivalent circuit, as described in the LEVM/LEVMW

manual **[38]** which is a composite circuit consisting of descrete, distributted dielectric (bulk) and conductive elements representative of our data. Six free parameters were used to obtain a good fit while the other parameters were fixed. The results show that the estimated χ^2 (chi-square) value is $5.4079 \cdot 10^{-4}$, the standard deviation (SD) is $2.3248 \cdot 10^{-2}$ and the fit quality factor is $-3.11 \cdot 10^{2}$, all of which are indices conveying a good fit. Analysis of the correllation matrix also shows valid results. The estimated relative standard deviation (RSD), which is an overall indicator of fit for the free parameters are all within $4.357 \cdot 10^{-3}$ to $6.956 \cdot 10^{-2}$, which are within the validity limits of a good fit (RSD≤ 0.2). **Fig. 11a** is a plot of the fit and experimental data using the 'O' model equivalent circuit (blue continuous line is the fit while the red squares are the experimental data points). Similar fitting results were obtained using the 'O' circuit for temperatures 500, 400 and 300 K.

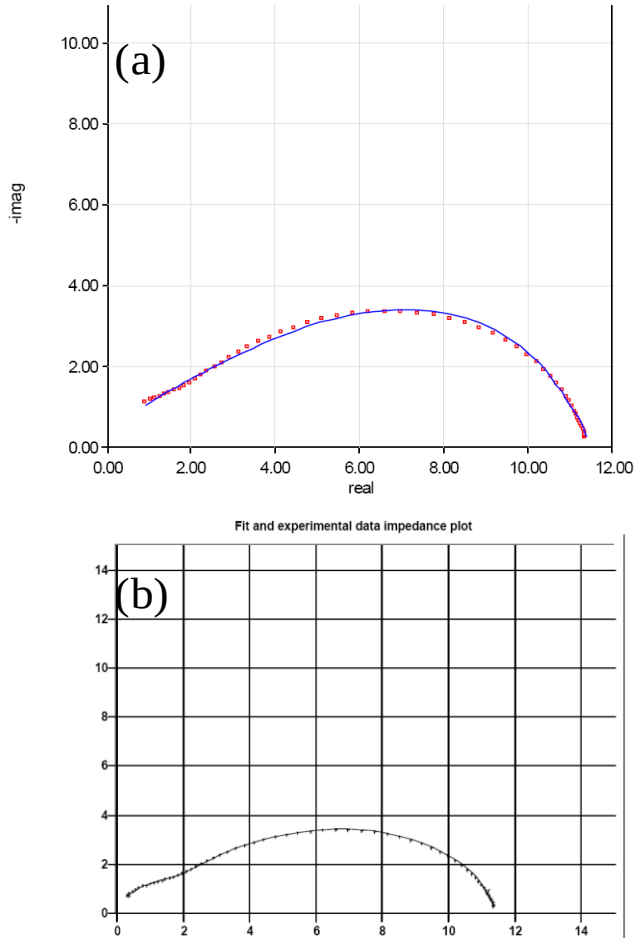

Fig. 11 (a) Plot of fit and experimental data using the 'O' model equivalent circuit and (b) typical result of the fit and experimental data ($-z''$ *vs* z') using the generic battery model for 600 K. The fit is the continuous line while the observed data are crosses.

Generic Battery model fitting

One of the potential applications of NASICON is in solid electrolytes, in lithium ion rechargeable batteries. In this case the present compound is the electrolyte. Li^+ ion is predominantly the conducting species in such compounds due to its light weight, making it suitable for applications in rechargeable lithium ion batteries. We have similarly fitted the data at selected temperatures (300, 400, 500 and 600 K) to a generic battery model (model circuit and empirical function) based on standard parameters of a Li^+ ion battery model using the MEISP program. Analysis shows the model fitted the data at the designated temperatures.

The generic battery model covers all kinetic steps relevant to electrochemical power sources which allows the comparison of qualitative kinetic processess of different battery types with eachother.The model is valid for both time and frequency domain processes. Details of generic battery model, circuit and empirical functions have been discussed in the MEISP program manual **[39]**. We have analysed the capacitive and resistive (impedance) variations with temperature earlier and now they would be viewed within generalized battery parameters.

Some of the parameters that affect the capacitive and resistive aspects of battery kinetic processes include, but not limited to, depth of battery discharge in % (DOD), resistance of separator and current collectors (R_{ser}), resistance of pasivating layer on particles (R_l), charge transfer resistance (R_{ct}), distributted resistance of transmission line representing electronic and ionic conduction inside the layer of active material (R_m) and resistance of new phase growth inside the particles (R_{ph}). Our data analysis is based on the resistive and capacitive variables for illustration.

In **Fig. 11b**, a typical result is provided for the fit and experimental data ($-z'', z'$) using the generic battery model for 600 K. The fit is the continuous line while the observed data are crosses. The fit parameters are valid in terms of their values, being typical for good fits and are observable by visual inspection. The fits are adequate both at low and high frequencies (frequency increases in an anticlockwise direction).

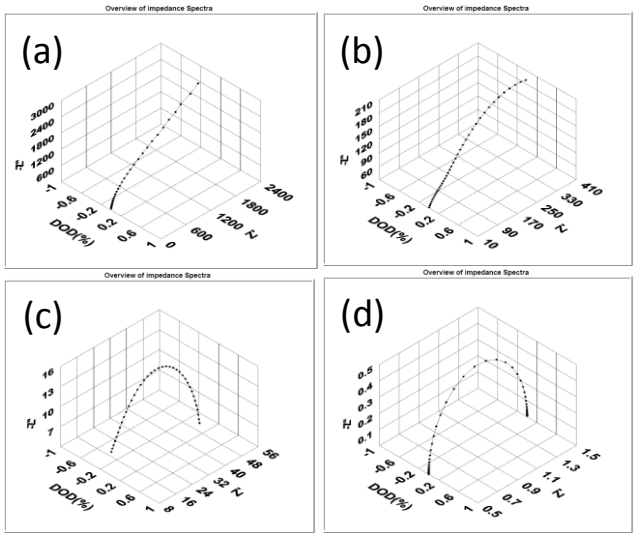

Fig. 12. 3D plots of the complex impedance vs % DOD at different temperatures: (a) 300, (b) 400, (c) 500 and (d) 600 K.

Fig. 12(a-d) are the 3D plots ($-z'', z''$) of the complex impedance vs % DOD at different temperatures (300 to 600 K). The % DOD remained virtually the same

throughout the temperature range, except at 500 K where there is a slight decrease. The relevant parameters involved in the dynamics of the kinetic processes are shown in fig. 13(a), where R_l and R_m are dominant. The other paramaters play negligible roles, though R_d is not negligible but small. Examination of the results of this fitting show that the RSD for the relevant parameters are $2.2017 \cdot 10^{-2}\Omega$ (R_l) and $2.735 \cdot 10^{-2}\Omega$ (R_m) and are indicative of good indices of a fit. Note that the light blue lines in the plots are the prefit results.

In **Fig. 13(b-c),** a typical battery model discharge file (within the generic battery model) was used to simulate the open circuit voltage (V) vs capacity (mAh) and storage capacitance (C_s) in Farads vs % DOD characteristics. The voltage is seen to drop slowly with increase in capacity to a point in which there is a sharp fall. On the otherhand, the C_s increased to a maximum and then decreased to zero at full discharge (100% DOD). The C_s vs % DOD plot for the different temperatures suggest that the the peaks of the % DOD successively shift toward higher % DOD (~ 60%) with increase in temperature.

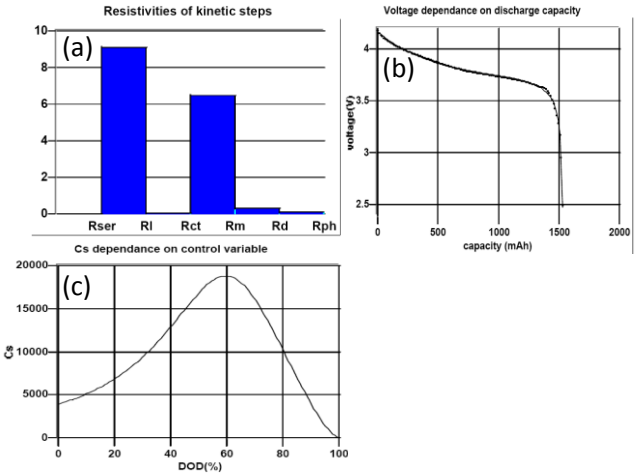

Fig. 13. Relevant parameters involved in the dynamics of the kinetic processes : (a) resistivities of the kinetic steps, (b) voltage dependence on discharge capacity and (c) storage cpacitance, C_s dependence on control variable. R_l and R_m are dominant and the other paramaters play negligible roles, though R_d is not negligible but small.

Analysis of the results of other temperatures shows that the kinetic processes involved change with temperature. For example at 400 K almost all the parameters are contributing, except $R_{ser,}$ whereas at 300 K only R_d is relevant and contributing.

Although different equivalent circuits have been used in the theoretical, CNLS and MEISP fitting procedures they all lead to good fits, nevertheless. This is due to the inherent ambiquities in getting an equivalent circuit as many would be equivalent if the values of the elements constituting the circuit were changed, and the fact that lumped-constant elements in the circuits can always be replaced by distributted elements which usually enhance the fitting results **[40]**.

Conclusion

The electrical condcutivity and dielectric behaviour of $Na_{0.25}Li_{0.75}Zr_2(PO_4)_3$ was investigated in the GHz range of frequency using a model RC circuit.The observed activation energies for the grain boundary and bulk were ~ 0.40 eV and 0.36 eV, respectively. Similarly, the maximum conductivity obtained for the bulk was 0.3 S/m, which comapares favouarably with typical NASICON materials. The dielectric permitivity ε' showed a non Debye behaviour and has maximum value of 136, which is high in comparison with most reported values for this family of compounds. Complex non linear least squares fitting results indicate a good fit to composite equivalent circuit parameters. Moreover, further fitting using the generic battery model suggests the material could be potential solid electrolyte material for lithium ion rechargeable battery applications due to the quality of the fitting paramaters obtained.

Acknowledgement

The authors express their profound appreciations to Dr. J. Ross Macdonald, William R. Kenan Jr. Professor of Physics, Emeritus; Department of Physics and Astronomy, University of North Carolina at Chapel Hill, and member of NAS and NAE, for finding time, despite his tight schedules to analyse some of the impedance data for this work, using the CNLS program LEVM/LEVMW developed by him.

Reference

1. Singh, N. K.; Pritam, K.; Radheshyam, Rai; Andrei, L. K**.** *Adv. Mat. Lett*. **2012**, 3, 315-320. **DOI**: 10.5185/amlett.2011.9305
2. Meera, R.; Yadav, K.L; Amit, K.; Piyush, K. P.; Nidhi, A.; Jyoti, R. *Adv. Mat. Lett***. 2012**, 3, 286-292. **DOI**: 10.5185/amlett.2012.2322.
3. Chamola, A.; Singh, H.; Naithani, U.C. *Adv. Mat. Lett*. **2011**, 2, 148-152. **DOI**: 10.5185/amlett.2010.11183
4. Singh, N.K.; Kumar, P.; Rai, R. *Adv. Mat. Lett.* **2011**, 2, 200-205. **DOI**: 10.5185/amlett.2010.11178
5. Sharma, S.; Rai, R.; Hall, D.A.; Shackleton, J. *Adv. Mat. Lett.* **2012**, 3, 92-96. **DOI**: 10.5185/amlett.2011.6279
6. Sahoo, S.; Pradhan, D. K.; Choudhary, R. N. P.; Mathur, B. K. *Adv. Mat. Lett.* **2012**, 3, 97-101. **DOI**: 10.5185/amlett.2011.4250
7. Zhang, A.;Yang, P.; Cao,Y.; Zhu,Y. *Adv. Mat. Lett.* **2011**, 2, 322-326. **DOI**: 10.5185/amlett.2011.3042am2011
8. Singha, N. K. ; Kumara, P.; Kumara, H.; Rai, R. *Adv. Mat. Lett.* **2010**, 1, 79-82. **DOI**: 10.5185/amlett.2010.3102
9. Mittal, R.; Singh, D. *Adv. Mat. Lett.* **2012**, 3, 38-43. **DOI**:10.5185/amlett.2011.5258
10. Mohantya, B. B. ; Sahooa, P. S. ; Sahoob, M. P. K.; Choudhary, R. N. P. *Adv. Mat. Lett.* **2012**, 3, 305-308. **DOI**: 10.5185/amlett.2011.11317
11. Tiwari, A.; Mishra, A.K.; Kobayash, H.; Turner, A. P. F.(Eds.) In *Intelligent Nanomaterials*; Wiley-Screviner, LLC USA, ***2012.***
12. Angadi, B.; Jali, V. M.; Lagare, M. T.; Kini, N. S.; Umarji, A. M.; Kumar, R.; Arora, S. K.; Kanjilal, D. *Nuc. Inst. Meth. Phys. Res. B* **2002,** 187, 87–94. **DOI:**10.1016/S0168-583X(01)00847-3
13. Kormaneni, S.; Lenain, E.; Roy, R. *J. Mater. Sci. Lett.* **1986,** 5, 1-3. **DOI:** 10.1007/BF01671415
14. Donald, I. W.; Metcalfe, B. L.; Taylor. R. N. J. *J. Mater. Sci.* **1997,** 32, 5864. **DOI:** 10.1023/A:1018646507438
15. Kang, H.; Cho, N. *J. Mater. Sci.* **1999,** 34, 5005-5013. **DOI:** 10.1023/A:1004784327302
16. Mouahid, F. E.; Zahir, M.; Maldonado-Manso, P. M.; Bruque, S.; Losilla, E. R.; Aranda, M. A. G.; Rivera, A.; Leona, C.; Santamaria, J. *J. Mater. Chem.* **2001,** 11, 3258-3263. **DOI:** 10.1039/b102918p
17. Oda, K.; Takase, S.; Shimizu, Y. *Materials Science Forum*, **2007,** 544-5 1033-1036.

DOI:10.4028/www.scientific.net/MSF.544-545.1033.
18. Tantri, P. S.; Greetha, K.; Umarji, A. M.; Ramasesha, S. K. *Bull. Mater. Sci.* **2000,** 23, 491-499. **DOI:** 10.1007/BF02903889
19. Petkov, V. I.; Orlova, A. I.; Trucbach, I. G.; Asabina, Y. A.; Demarin, V. T.; Kurazhkovskaya, V. S. *Czech. J. Phys.* **2003,** 53, A639-A648.
20. Aono, H. 1994, PhD Thesis, Osaka University, Japan.
21. Venckute, V.; Banyte, J.; Kazlauskiene, V.; Miškinis, J.; Šalkus, T.; Kežionis, A.; Kazakevi˘cius, E.; Dindune, A.; Kanepe, Z.; Ronis, J.; Orliukas, A. F. *Lithuanian J. Phys.* **2010,** 50, 435–443. **DOI:** 10.3952/lithjphys.50403
22. Salkus, T.; Kezionis, A.; Dindune, A.; Kanepe, Z.; Ronis, J.; Miskinis, J.; Kazlauskiene, V.; Gauckler, L. J.; Pmucke, U.; Orliukas, A. F. *J. Phys. : Condens. Matter.* **2007,** 19**,** 106204.
23. Chae-Myung, C.; Seong-Hyeon, H.; Hyun-Min, P. *Solid State Ionics*, **2005,** 176, 2583– 2587. **DOI:** 10.1016/j.ssi.2005.07.010
24. Anantharamulu, N.; Prasad, G.; Vithal, M. *Bull. Mater. Sci.* **2008,** 31, 133–138. **DOI:** 10.1007/s12034-008-0023-3
25. Salkus, T.; Dindune, A; Kanepe, Z.; Ronis, J.; Kazeonis, A.; Orliukas, A. E. *Lithuanian J. Phys.* **2006,** 46, 361-366. **DOI:** 10.3952/lithjphys.46314
26. Ahmadu, U.; Musa, A. O.; Jonah, S. A.; Rabiu, N. *J. Therm. Anal. Cal.* **2010,** 101, 175-179. **DOI:** 10.1007/s10973-010- 0679-y
27. Ahmadu, U.; Ŝalkus, T.; Musa, A. O.; Isah, K. U. *Open Journal of Physical Chemistry* **2011,** 1, 94-103 **DOI:** 10.4236/ojpc.2011.13013.
28. Tomas,. Ŝ., Dindune, A;Kanepe, Z; Ronis, J.; KaŽeonis, A; Orliukas, A.E. *Lithuanian Journal of Physics.* 2006, 46, 361-366. **DOI:** 10.3952/lithjphys.46314
29. Koteswara, R. K.; Rambabu, G.; Raghavender, M.; Prasad, G.; Kumar, G. S.; Vithal, M.; *Solid State Ionics* **2005,** 176, 2701-2710. **DOI:** 10.1016/j.ssi.2005.07.016
30. Leo, C. J.; Rao, G. V. S.; Chowdari, B. V. R. *J. Mater. Chem.* **2002,** 12, 1848–1853. **DOI:** 10.1039/b110863h
31. Gosh, A. *Phy. Rev. B* **1990,** 42, 1388-1393. **DOI:** 10.1103/PhysRevB.42.1388
32. Jarboui, A.; Ben Rhaeim, A.; Hilel, F.; Guidara, K.; Gargouri, M. *Ionics* **2010,** 16, 67–73. **DOI:** 10.1007/s11581-009-0333-5
33. Vitioo, I. 1999, PhD Thesis. Inst. of Solid State Physics, University of Latvia.
34. Liu, J.; Chun-Gang, D.; Wei-Guo, Y.; Mei, W. N.; Smith, R. W.; Hardy, J. R. *Phy. Rev. B* **2004,** 70, 144106. **DOI:** 10.1103/PhysRevB.70.144106
35. Shaisha, E. E.; El-Desouki Sh, F.; Shaltout, I.; Bahgat, A. A. *J. Mater. Sci. Technol.* **2006,** 22, 701-707.
36. Sharma, M. V. N. V. D.; Sarma, A. V.; Rao, R. B. *Turk. J. Phys.* **2009,** 33, 87 – 100 **DOI:** 10.3906/fiz-0803-7.
37. Salkus, T.; Kazakevi˘cius, E.; Ke˘zionis, A.; Dindune, A.; Kanepe, Z.; Ronis, J.; Emery, J.; Boulant, A.; Bohnke, O.; Orliukas, A. F. *J. Phy. Condens. Matter* **2009,** 21, 185502. **DOI**: 10.1088/0953-8984/21/18/185502
38. Macdonald, R. *Complex Nonlinear Least Squares, Immittance, Inversion, and Simulation Fitting Programs* for WINDOWS and MS-DOS LEVM / LEVMW Manual, Version 8.11 (October, 2011).pp.5-29/30.
39. MEISP, March, 2002.Korea: Kumho Chemical Laboratories, 2002.
40. Macdonald, J. R.; Johnson, W. B. (2005). Fundamentals of impedance spectroscopy. *In* Barsoukov, E. ; Macdonald, J.R.(Eds.), *Impedance spectroscopy theory,experiment, and applications*, second edition. A John Wiley & Sons, Inc., Publication, Hoboken, New Jersey, U.S.A. pp. 9-11.

